THE ASTRONOMICAL JOURNAL VOLUME 108, NUMBER 5 NOVEMBER 1994

TWO VIEWS OF THE ANDROMEDA GALAXY Hα AND FAR INFRARED

NICHOLAS A. DEVEREUX
Department of Astronomy, New Mexico State University, Las Cruces, New Mexico
Electronic mail: devereux@nmsu.edu

ROB PRICE
Department of Physics & Astronomy, University of New Mexico, Albuquerque, New Mexico

LISA A. WELLS
Kitt Peak National Observatory, National Optical Astronomy Observatories, Tucson, Arizona
Electronic mail: lwells@noao.edu

NEB DURIC
Department of Physics & Astronomy, University of New Mexico, Albuquerque, New Mexico
Electronic mail: duric@deneb.unm.edu

Received 1994 May 4; revised 1994 June 24

ABSTRACT

A complete Hα image of the Andromeda Galaxy (M31) is presented allowing the first direct measurement of the total Hα luminosity which is $(7.3\pm2.4)\times10^6 L_\odot$. The H$\alpha$ emission is associated with three morphologically distinct components; a large scale star-forming ring, $\sim$1.65° in diameter, contributing 66% of the total Hα emission, a bright nucleus contributing 6% of the total Hα emission with the remaining 28% contributed by a previously unidentified component of extended and filamentary Hα emission interior to the star forming ring. The correspondence between the Hα image and the *IRAS* far-infrared high resolution image is striking when both are convolved to a common resolution of 105 arcsec. The close correspondence between the far-infrared and Hα images suggests a common origin for the two emissions. The star-forming ring contributes 70% of the far-infrared luminosity of M31. Evidence that the ring emission is energized by high mass stars includes the fact that peaks in the far-infrared emission coincide identically with H II regions in the Hα image. In addition, the far-infrared to Hα luminosity ratio within the star-forming ring is similar to what one would expect for H II regions powered by stars of spectral types ranging between O9 and B0. The origin of the filamentary Hα and far-infrared luminosity interior to the star-forming ring is less clear, but it is almost certainly not produced by high mass stars.

1. INTRODUCTION

Developing an empirical measure of the current high mass star-formation rate in spiral galaxies is central to predicting the future evolution of the Hubble Sequence. Methods used to measure high mass star-formation rates include the Hα luminosity (e.g., Kennicutt & Kent 1983), the UV luminosity (e.g., Donas *et al.* 1987), and the far-infrared luminosity (e.g., Devereux & Young 1991). None of the aforementioned methods provide a perfect measure of the current high mass star-formation rate. Nevertheless, it is important to understand the nuances of each so that conclusions based on a particular tracer may be interpreted within the context of its limitations.

The Hα emission line luminosity in principle provides the most direct measure of the high mass star-formation rate because it originates from the ionized region directly surrounding high mass stars. In practice, however, the Hα emission line suffers from extinction. Besides, Hα measurements exist for only $\sim$200 galaxies at present (Kennicutt & Kent 1983; Romanishin 1990; Kennicutt 1992; Ryder & Dopita 1993). Consequently, statistical studies of high mass star-formation rates for spiral galaxies of different Hubble type are limited by small numbers. High mass stars also produce UV emission but use of the UV luminosity to measure high mass star-formation rates is also compromised by extinction and, in the early type spiral galaxies, by an as yet unidentified source of UV emission in spiral bulges (Code *et al.* 1972; Bohlin *et al.* 1985; Burstein *et al.* 1988; O'Connell *et al.* 1992). Additionally, like Hα, statistical studies that utilize UV measurements are limited by small numbers (Donas *et al.* 1987; Kodaira *et al.* 1990). By far the most statistically complete database of measurements for spiral galaxies is provided by the Infrared Astronomical Satellite (*IRAS*), but interpretation of the *IRAS* data in the context of high mass star-formation rates continues to be hampered by the lingering controversy surrounding the origin of the far-infrared luminosity. The controversy centers on whether the far-infrared luminosity is powered primarily by ionizing stars (Young *et al.* 1984; Helou *et al.* 1985; Rengarajan & Verma 1986; Sanders *et al.* 1986; Gavazzi *et al.* 1986; Leech *et al.* 1988; Devereux & Young 1990, 1991, 1992, 1993; Price & Duric 1992; Devereux & Scowen 1994) or nonionizing stars (Lonsdale-Persson & Helou 1987; Walterbos & Schwering

1987; Bothun *et al.* 1989; Bothun & Rogers 1992). Some have suggested contributions from both (Smith 1982; Habing *et al.* 1984; Rice *et al.* 1990; Smith *et al.* 1991) that may depend on Hubble type (Sauvage & Thuan 1992). The *IRAS* measured far-infrared fluxes for literally thousands of galaxies (Cataloged Galaxies & Quasars in the *IRAS* Survey 1985). It is therefore particularly important to determine to what extent the far-infrared luminosity can be used to measure high mass star-formation rates so that the *IRAS* database can be exploited to its full potential.

M31 has frequently been the focus of the controversy surrounding the origin of the far-infrared luminosity. The earliest study based on the *IRAS* data (Habing *et al.* 1984) associated the ring emission with O and B stars, on the grounds that "maxima in the 60 μm map coincide almost without exception with areas of large and bright H II regions." Walterbos & Schwering (1987), on the other hand, concluded that less than 10% of the far-infrared luminosity is produced by O and B stars, the bulk of the far-infrared emission being attributed to diffuse dust heated by the general interstellar radiation field of nonionizing stars, more commonly referred to as "cirrus." Since Walterbos & Schwering (1987), M31 has long been upheld as an example of a galaxy for which the far-infrared luminosity is dominated by cirrus and consequently evidence that the far-infrared luminosity may not be a reliable measure of the high mass star-formation rate, at least in early type spirals. However, the new results presented here provide significant grounds for revision of the widely accepted wisdom concerning the origin of the far-infrared luminosity in M31. The revision is based on new far-infrared and Hα images that have become available following two recent developments. The first is the application of a high resolution reconstruction algorithm that improved the resolution of the *IRAS* data for M31 by about a factor of 2 (Aumann *et al.* 1989). The second development was the arrival of a 2048×2048 CCD chip at the Burrell Schmidt telescope at Kitt Peak that allowed the central ~2 degree region of M31 to be imaged in only two fields. The ability to compare *maps* of the far-infrared and Hα luminosity has proven to be a useful technique for constraining the origin of the far-infrared luminosity in the *late* type spiral galaxies M51 (Devereux & Young 1992), NGC 6946 (Devereux & Young 1993), and M101 (Devereux & Scowen 1994). The technique is extended here to include the *early* type spiral galaxy M31. Comparison of far-infrared and Hα maps is particularly advantageous for elucidating the origin of the far-infrared luminosity within M31 because at a distance of 0.7 Mpc, it is the nearest and consequently the best resolved spiral galaxy.

The new imaging observations are described in Sec. 2 along with a brief review of the *IRAS* data for M31. The results are presented in Sec. 3 and discussed in Sec. 4 within the context of the origin of both the far-infrared and Hα emission within M31. The conclusions are presented in Sec. 5.

2. THE DATA

2.1 The Hα Images

The new Hα images of M31 were obtained with the Case Western Burrell Schmidt telescope at Kitt Peak National Observatory during the night of 1993 November 9. The inner two degrees of M31 were imaged at 2 arcsec resolution in two fields with considerable overlap in the nuclear region. Hα+[N II] emission line plus continuum images were obtained using a narrow, 74 Å, filter centered at 6568 Å, and continuum subtracted using images obtained with a narrowband, 72 Å, line free continuum filter centered at 6481 Å. Three 15 min exposures were obtained through each filter at each of the two positions imaged. The images were bias subtracted, flatfielded, registered, median combined, and sky subtracted. The continuum image was scaled and subtracted from the line plus continuum image to remove the foreground stars and the galaxy stellar continuum emission. The two emission line only images were then mosaiced together to produce the picture presented in Fig. 1 [Plate 77].

Figure 1 reveals three morphologically distinct components for M31 including a large star-forming ring that is 1.65° in diameter, extended and filamentary Hα emission interior to the ring that is centered on a bright nuclear spiral. The existence of the star-forming ring has been known for many years (Baade & Arp 1964; Pellet *et al.* 1978). The nuclear spiral was discovered more recently by Jacoby *et al.* (1985).

2.2 The IRAS HiRes Images

The *IRAS* 60 and 100 μm HiRes images were generated by the staff of the Infrared Processing & Analysis Center (IPAC). The resolution of the HiRes 60 μm images is higher than that of the 100 μm data due to the different detector sizes. It is extremely important, however, when combining the *IRAS* 60 and 100 μm images to produce maps of the far-infrared luminosity to convolve the 60 and 100 μm data to the same resolution. To this end, the HiRes resolution maps were inspected to determine the beam profiles at 60 and 100 μm. The resolution maps were then convolved with a variety of kernels until the 60 and 100 μm beams were circularized with a diameter of 105 arcsec. The convolution procedure was then repeated on the 60 and 100 μm images of M31.

Following convolution to a common resolution of 105 arcsec the HiRes 60 and 100 μm images were linearly combined into a far infrared luminosity L(FIR) image using the following relation:

$$L(\mathrm{FIR})=3.65\times10^5 S(\mathrm{FIR})D^2$$

(Cataloged Galaxies & Quasars in the *IRAS* Survey 1989) where $S(\mathrm{FIR})=2.58\ S(60\ \mu\mathrm{m})+S(100\ \mu\mathrm{m})$ and L(FIR) approximates the luminosity that would be measured in a filter 40–120 μm wide. An image showing the spatial distribution of far-infrared luminosity within M31 is presented in Fig. 2 [Plate 78], along with the Hα image convolved to the same 105 arcsec resolution.

3. RESULTS

3.1 Comparison of the Far-Infrared and Hα Morphology

The similarity between the spatial distribution of the far-infrared luminosity, L(FIR), and the Hα luminosity, L(Hα), within M31 is striking (see Fig. 2). Almost every feature in the *IRAS* HiRes far-infrared image has a counterpart in the Hα image. There is one notable exception, however, the bright patch of far-infrared emission 4.8 arcmin to the northwest of the nucleus has no counterpart in the Hα image. A detailed analysis of the individual *IRAS* detector scans by John Fowler at IPAC suggests that the far-infrared feature is real. The issue will not be fully resolved however until the region is mapped again, either from the Kuiper Airborne Observatory or the Infrared Space Observatory. The most important difference between the far-infrared and Hα images, however, is that the far-infrared emission appears to be more diffuse than the Hα emission, particularly within the star-forming ring. The difference is unlikely to be due to resolution effects because both images have been convolved to a common resolution of 105 arcsec. An explanation for the difference will be presented in Sec. 4. Measurements of the far-infrared and Hα luminosity that is associated with each of the three primary morphological components; namely the large scale star-forming ring, the nucleus, and the extended filamentary emission, will be presented in the following section.

3.2 The Hα Fluxes and Luminosities

The Hα emission line images were flux calibrated using images of the standard star BD+28 4211 (Massey *et al.* 1988) that were obtained on the same night as the M31 observations. A number of tests have been performed to evaluate the reliability of the flux calibration. The first test was to determine the relative calibration between the two emission line images that were mosaiced together to produce the complete image presented in Fig. 1. The nucleus of M31 appears in both images and the Hα flux agrees to within 10%. A number of H II regions are common to both images and their Hα fluxes also agree to within 10%. We have also compared Hα fluxes for H II regions that were imaged independently by Walterbos & Braun (1992). Our fluxes tend to be ~20% higher on average than those of Walterbos & Braun (1992) but consistent with the brightening expected from the inclusion of the [N II] emission line in our measurements. The Hα flux measured for the nuclear region has also been compared with an independent measurement by Jacoby *et al.* (1985). The extinction corrected flux of 3.2×10^{-11} ergs cm^{-2} s^{-1} reported by Jacoby *et al.* (1985) for the central 235×235 arcsec^2 region of M31 has been reddened by A_V=0.33 mag to 2.54×10^{-11} ergs cm^{-2} s^{-1} in order to facilitate comparison with the new observations reported here. The Hα emission line flux of $(3.2\pm0.9)\times10^{-11}$ ergs cm^{-2} s^{-1} that we measure in the central 235×235 arcsec^2 region is about 25% higher than that reported by Jacoby *et al.* (1985). However, Jacoby *et al.* caution that their flux may be a lower limit if the background level that they subtracted included a contribution from a component of extended Hα emission. The existence of such a component of extended Hα emission is confirmed by our observations.

The Hα emission extending from the nuclear spiral is filamentary and morphologically distinct from the Hα emission in the star-forming ring. Hα filaments can be traced from the nuclear spiral to 2 or 3 kpc along the major axis. The filaments remain remarkably coherent despite the fact that they change position angle by as much as 90° or more. Particularly impressive are the filaments that extend from the eastern side of the nuclear bar northeast along the major axis and the filament that extends from the western end of the nuclear bar southeast along the minor axis (see Fig. 1).

There are two primary sources of uncertainty in determining absolute Hα fluxes for M31. The first is systematic and relates to the level of the continuum that is subtracted from the line plus continuum images, the second is random and relates to the noise in the image caused by residuals from incompletely subtracted foreground stars.

The continuum level was determined by measuring the counts for several stars common to both the continuum and line plus continuum images, taking the ratio of the counts, averaging the ratio for several stars and scaling the continuum image to the line plus continuum image so that the average ratio is unity. The dispersion in the average ratio was typically 3% and representative of the uncertainty in the determination of the continuum level. Unfortunately, the Hα fluxes are very sensitive to the level of the continuum subtracted from the line plus continuum images. The uncertainty in the Hα fluxes due to a plausible ±3% uncertainty in the continuum level was determined empirically to be ±10% for the star-forming ring, ±50% for the filamentary emission interior to the ring, and ±30% for the nucleus. The second source of error is related to the noise caused by residuals from incompletely subtracted foreground stars. Very slight differences between the profiles of stars in the continuum and line plus continuum images make it virtually impossible to completely remove the considerable number of foreground stars from the Hα emission line image of M31. The noise from incompletely subtracted stars limits the 1σ sensitivity to 4×10^{-17} ergs cm^{-2} s^{-1} pixel^{-1} and results in a combined 1σ uncertainty of ±25% for the star-forming ring, ±13% for the diffuse emission interior to the ring, and ±1% for the nuclear emission.

The Hα fluxes that we obtain for the three principal morphological components of M31 are listed in Table 1 and have not been corrected for extinction or [N II] emission. The uncertainties reflect the quadrature sum of the systematic and random errors described above. The total Hα luminosity of M31 was measured within an elliptical region centered on the nucleus with a major axis of 114.25 arcmin, a minor axis of 36 arcmin, and rotated to a position angle of 40°. The Hα luminosity associated with the extended and filamentary emission interior to the star-forming ring was measured within an elliptical region centered on the nucleus with a major axis of 55 arcmin, a minor axis of 15 arcmin, and rotated to a position angle of 45°. The Hα luminosity associated with the star-forming ring was taken to be the differ-

TABLE 1. Fluxes and luminosities for the principal morphological components of M31.

Region	F(Hα) 10^{-10} erg cm^{-2} s^{-1}	L(Hα) 10^{6} $L_{\odot}$	S(FIR) Jy	L(FIR) 10^{8} $L_{\odot}$
(1)	(2)	(3)	(4)	(5)
Star Forming Ring	3.29 ± 0.86	4.77 ± 1.25	2864 ± 288	10.80 ± 1.1
Diffuse Emission[a]	1.44 ± 0.74	2.09 ± 1.07	983 ± 100	3.70 ± 0.3
Nuclear Emission[b]	0.32 ± 0.09	0.47 ± 0.14	140 ± 12	0.53 ± 0.04
Total	5.05 ± 1.69	7.33 ± 2.46	3987 ± 399	15.0 ± 1.5

Notes to TABLE 1

The uncertainties reflect random errors due background noise in the images in addition to continuum subtraction uncertainties for the Hα fluxes and a ± 10% calibration uncertainty for the IRAS fluxes.

[a]Diffuse Emission interior to the star forming ring but not including the nuclear 235 arc second square region.

[b]Nuclear 235 arc second square region.

ence of the luminosities measured within the two elliptical regions defined above.

The total observed Hα luminosity, integrated over the central 1.65° diameter region, is $(7.3\pm2.4)\times10^6\ L_\odot$ which is about a factor of 2 larger than that estimated by Walterbos & Braun (1994) based on a partial map of M31. We expect our estimate of the total Hα luminosity to be more reliable, however, due to the fact that we imaged essentially the entire galaxy. Approximately 66% of the total Hα luminosity is contributed by the large scale star-forming ring, the remaining 34% is associated with the nucleus and a more extended component of filamentary Hα emission. The Hα luminosity measured for the central 235 arcsec^2 region, imaged previously by Jacoby *et al.* (1985), is $(4.7\pm1.4)\times10^5\ L_\odot$ and represents only 6% of the total Hα luminosity of M31.

3.3 The Far-Infrared Fluxes and Luminosities

The far-infrared fluxes and luminosities of the principal morphological components in M31 are listed in Table 1 and refer to exactly the same regions for which the Hα fluxes and luminosities were measured. Obviously the dust responsible for the far-infrared luminosity of M31 radiates longward of 100 μm even though the *IRAS* detectors were unable to measure the long wavelength emission. A lower limit to the total (40–1000 μm) luminosity may be estimated by assuming that the spectral energy distribution of M31 is represented by a single temperature blackbody fitted to the global *IRAS* 60 and 100 μm fluxes. The global *IRAS* 60 and 100 μm fluxes of M31 indicate a dust color temperature of 26 K for a λ^{-1} emissivity law in which case the 40–120 μm luminosity measured by *IRAS* represents about 47% of the total 40–1000 μm luminosity. Consequently, the 40–120 μm luminosities measured by *IRAS* have been scaled up by a factor of 2.11 to provide a more accurate measure of the total (40–1000 μm) far-infrared luminosity radiated by M31. The measurements provided in Table 1 show that the total (40–1000 μm) far-infrared luminosity of M31 is $(1.5\pm0.15)\times10^9\ L_\odot$ in good agreement with previous determinations by Walterbos & Schwering (1987) and Rice *et al.* (1988). The low far-infrared luminosity of M31 places it at the low end of the far-infrared luminosity function for early type spiral galaxies (Devereux & Young 1991). The spatial distribution of far-infrared luminosity within M31 is remarkably similar to the Hα luminosity with approximately 71% of the total far-infrared luminosity associated with the star-forming ring and the remaining 29% contributed by the nucleus and a more extended component of diffuse far-infrared emission interior to the star-forming ring.

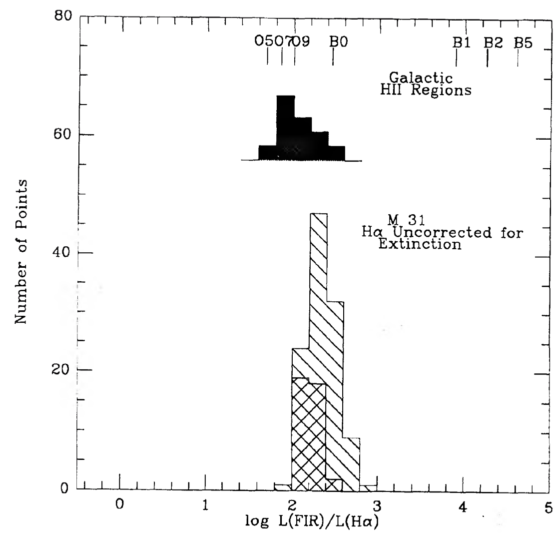

FIG. 3. Histogram showing the distribution of L(FIR)/L(Hα) ratios measured with a circular beam 180 arcsec in diameter at 114 independent locations within M31. The single hatched histogram pertains to the star-forming ring, the double hatched histogram to the nucleus and associated filamentary emission interior to the star-forming ring. The distribution of L(FIR)/L(Hα) ratios inferred for Galactic H II regions is also shown for comparison.

4. DISCUSSION

4.1 The Origin of the Luminosity in the Star-Forming Ring

The visual impression provided by Fig. 2, that the spatial distribution of far-infrared luminosity is similar to the Hα luminosity, is quantitatively confirmed by the results presented in Table 1. The majority (~70%) of both the far-infrared and Hα luminosity of M31 is associated with the star-forming ring. The peaks in the far-infrared image coincide with peaks in the Hα image suggesting H II regions as the origin of both the far-infrared and Hα luminosity. The association is further supported by measurements of the L(FIR)/L(Hα) ratios. The histograms shown in Fig. 3 represent the distribution of L(FIR)/L(Hα) ratios measured at 114 independent locations within M31. The resolution of the measurements is 180 arcsec corresponding to a linear resolution of 630 pc at the distance of M31. The corresponding distribution of L(FIR)/L(Hα) ratios determined for Galactic H II regions (Devereux & Scowen 1994) is also shown for comparison. The distribution of ratios measured at the location of the star-forming ring, is depicted by the single hatched histogram. The double hatched histogram pertains to the nucleus and its associated component of extended emission and will be discussed further in the next section.

The distribution of $L(\mathrm{FIR})/L(\mathrm{H}\alpha)$ ratios is very narrow providing further testament to the excellent correlation between the far-infrared and Hα emission within M31. The median of the distribution of $L(\mathrm{FIR})/L(\mathrm{H}\alpha)$ ratios for the star-forming ring lies in between the values expected for H II regions powered by O9 and B0 stars. It is important to note that the Hα luminosity has not been corrected for extinction. Walterbos & Braun (1994) estimate $\tau_{\mathrm{H}\alpha}\sim1.25$ based on measurements of the H I column and a Galactic gas to dust ratio. Estimates of the extinction to H II regions that are based on measurements of the gas column are highly unreliable, however, because the gas column usually pertains to an average over a much larger region than that producing the Hα emission, as discussed previously by Devereux & Scowen (1994). Estimates of the extinction that are based on direct measurements of the ionized gas, such as the Balmer decrement or high angular resolution thermal radio continuum maps, are expected to be much more reliable. Such data are regrettably unavailable for M31, but application of such methods to measure the extinction to H II regions in other galaxies indicate A_V is typically 1–2 mag (Israel & Kennicutt 1980; Scowen *et al.* 1992). Correcting the Hα luminosity for a conservative 1 mag of visual extinction would shift the median of the distribution of $L(\mathrm{FIR})/L(\mathrm{H}\alpha)$ ratios measured for the star-forming ring in M31 to a value more indicative of H II regions powered by O9 stars. The histogram, in itself, does not prove that the far-infrared luminosity is supplied by O and B stars. A 50% contribution to the far-infrared luminosity from nonionizing stars, for example, would shift the histogram to the right by only 0.3 dex. The histogram merely supports the association of the far-infrared and Hα luminosity with O and B stars that is motivated by the striking correspondence between the far-infrared and Hα images of M31 presented in Fig. 2.

The thermal dust temperature within M31, derived from the global $S_{100\ \mu\mathrm{m}}/S_{60\ \mu\mathrm{m}}$ flux ratio, leads to a value of $\sim$26 K for a λ^{-1} emissivity law (23 K for a λ^{-2} emissivity law). The dust temperature inferred for M31 is unusually low compared to other spiral galaxies. Many investigators (Lonsdale-Persson & Helou 1987; Walterbos & Schwering 1987; Bothun *et al.* 1989) have attempted to use the dust temperature to estimate the high mass star-formation rate. The procedure involves separating the *IRAS* 60 and 100 μm emission into two dust temperature components; a warm $\sim$40–50 K dust component that is identified with H II regions and a cooler $\sim$16–20 K dust component that is identified with cirrus heated by nonionizing stars. Application of such a procedure led Walterbos & Schwering (1987) to the result that only 10% of the far-infrared luminosity of M31 is generated by high mass stars and subsequently to the conclusion that the far-infrared luminosity is a poor measure of the high mass star-formation rate. The result is clearly inconsistent with the new results presented here which indicate that the star-forming ring contributes $\sim$70% of the far-infrared luminosity. Evidently the dust temperature is a poor measure of the high mass star-formation rate, at least in M31.

As noted previously, the far-infrared emission in M31 appears to be more diffuse than the Hα emission, particularly within the star-forming ring. The far-infrared emission was also observed to be more diffuse than the Hα emission in the late-type spiral galaxy M101 which Devereux & Scowen (1994) attributed to the fact that the path length of the ionizing photons which give rise to the Hα emission is much shorter than the path length of the nonionizing photons that escape H II regions and primarily responsible for heating the dust. Such an explanation is equally applicable to M31.

4.2 The Origin of the Nuclear and Extended Filamentary Emission

The nuclear and associated extended filamentary emission interior to the star-forming ring contributes approximately 30% of the total far-infrared and Hα luminosity of M31. At high resolution, the Hα emission contained within the central 800 pc^2 region resolves into a bar and filamentary structure resembling spiral arms (see inset Fig. 1) as described previously by Jacoby *et al.* (1985). The new results illustrated in Fig. 1 show that the filamentary spiral structure can be traced much further to $\sim$2–3 kpc either side of the nucleus along the major axis direction. Although a number of possibilities have been discussed previously by Jacoby *et al.* (1985), Ciardullo *et al.* (1988) and references therein, a satisfactory explanation for the unusual morphology, the source of the ionization and the irregular kinematics for the gas in the center of M31 remains elusive. Lauer *et al.* (1993) present evidence, based on a Space Telescope image, that M31 hosts two nuclei suggesting that M31 cannibalized another galaxy. Perhaps the nuclear spiral is the vestige of the galaxy which M31 cannibalized. The unusual kinematics (Rubin & Ford 1971; Ciardullo *et al.* 1988) and the larger scale warped disk, that is evident in both the optical (Arp 1964) and H I (Henderson 1979), provide further evidence that M31 has participated in an interaction.

While the possibility that M31 may have recently cannibalized another galaxy may explain the double nucleus and the unusual morphology and kinematics of the neutral and ionized gas within M31, it is the origin of the energy source(s) that give rise to the considerable far-infrared and Hα luminosity interior to the star-forming ring that remains uncertain. The $L(\mathrm{FIR})/L(\mathrm{H}\alpha)$ ratio is marginally lower than that in the star-forming ring and similar to that expected for H II regions powered by O9 stars, but such stars are clearly not responsible for the far-infrared and Hα luminosity for several reasons. First, while the far-infrared and Hα luminosity observed interior to the star-forming ring could, in principle, be supplied by $\sim$10 000 O9 stars, the morphology of the Hα emission is filamentary and unlike that of the star-forming ring, and unlike that expected for H II regions. Furthermore, the stars identified in a Space Telescope image of the central 44 arcsec region of M31 (King *et al.* 1992) are much too faint to be O9 stars although they could be B5 stars. B5 stars would not be expected to generate large H II regions but the surface density of B5 stars that would be required to sustain the observed Hα luminosity exceeds the surface density of stars in the Space Telescope image by at least a factor of 200. Consequently, high mass stars; the most common source of ionizing radiation in spiral galaxies, appears to be ruled out as the primary cause for Hα emission interior to the star forming ring in M31. Jacoby *et al.* (1985) rule out Planetary Nebula as a source for the ionization and there is little evidence to suggest ionization by an active nucleus. Soifer *et al.* (1986) attribute the far-infrared luminosity to interstellar dust heated by the radiation field of the bulge stars, but the model provides no explanation for the ionized gas emission. Exploration of a more radical model, that appeals to the mechanical energy of the collision that may have given rise to the double nucleus, the nuclear spiral and the large scale warp in M31, is beyond the scope of the present paper, but was suggested previously by Harwitt *et al.* (1987) as a plausible mechanism for generating the far-infrared and ionized gas emission in colliding galaxies.

4.3 Which is the Better Measure of the High Mass Star-Formation Rate; the Hα or Far-Infrared Luminosity?

In the case of the star-forming ring, which dominates the total far-infrared and Hα luminosity of M31, the high mass star-formation rate derived from the far-infrared luminosity is, in principle, equivalent to that derived from the Hα luminosity for the reasons discussed in Sec. *4.1*. On the other hand, the nuclear and associated filamentary emission interior to the star-forming ring is clearly not powered by high mass stars for the reasons described in Sec. *4.2*. Unfortunately, the only way to distinguish the two components in M31 is on the basis of morphology as characterized by the high angular resolution Hα image. However, high angular resolution is a luxury not afforded for most galaxies because they are more distant than M31. In fact, for the majority of galaxies, angular resolution limitations permit measurement only of the *global* star-formation rate based on measurements of the global Hα or the global far-infrared luminosity. In the case of M31, the star-formation rate estimated from the *global* far-infrared luminosity would be the same as the star-formation rate estimated from the *global* Hα luminosity because the $L(\mathrm{FIR})/L(\mathrm{H}\alpha)$ ratio is indicative of H II regions at all locations (see Fig. 3), but *both would be overestimated by 30%* due to the filamentary emission interior to the star-forming ring that is clearly not associated with H II regions. Global star-formation rates estimated for other early type spiral galaxies that are based on measurements of the global far infrared and Hα luminosities may be similarly compromised. So the issue is not really whether the far-infrared luminosity is as good a measure of the high mass star-formation rate as the Hα luminosity but rather to what extent is each tracer compromised by emission from sources other than O and B stars. The results presented here indicate that the far infrared and Hα are similarly disadvantaged.

5. SUMMARY AND CONCLUSIONS

New imaging observations have permitted a measurement of the total Hα luminosity for the Andromeda Galaxy (M31). The total Hα luminosity is $(7.3\pm2.4)\times10^6\,L_\odot$. The H$\alpha$ luminosity of M31 is associated with three morphologically distinct components including a large scale star-forming ring that is $\sim$21 kpc in diameter and contributing $\sim$70% of the total Hα luminosity, a bright nucleus $\sim$1 kpc in diameter, and filamentary emission that extends 2–3 kpc along the major axis. The correspondence between the Hα image and the *IRAS* HiRes far-infrared image is striking when both are convolved to a common resolution of 105 arcsec. The coincidence suggests a common origin for the two emissions. The positional coincidence between the Hα and far-infrared emission peaks does not in itself prove that O and B stars are responsible for the far-infrared luminosity in the star-forming ring. However, when combined with the $L(\mathrm{FIR})/L(\mathrm{H}\alpha)$ ratios, which are indicative of the luminosity ratios expected for H II regions, it is difficult to argue that O and B stars are not responsible for the far-infrared luminosity, at least in the star-forming ring.

Even though M31 is one of the lowest luminosity early type spiral galaxies known, O and B stars appear capable of supplying $\sim$70% the total far-infrared and Hα luminosity that is associated with the star-forming ring. High mass stars are unable, however, to explain 30% of the total far-infrared and Hα luminosity that is associated with the filamentary emission interior to the star-forming ring. Consequently, the far-infrared luminosity is a reliable a measure of the high mass star-formation rate as the Hα luminosity, but both are equally compromised by emission that is not associated with H II regions.

It is a pleasure to acknowledge the assistance of NOAO staff in acquiring the Hα image of M31, Jeanette Barnes, Taft Armandroff, Ed Carder, and George Jacoby, in particular. N.D. gratefully acknowledges NASA for a Long Term Space Astrophysics Grant without which this work would not have been possible. The authors would like to thank Dr. Rene Walterbos for useful comments and suggestions. The Hα observations were obtained with the Burrell Schmidt telescope of the Warner and Swasey Observatory, Case Western Reserve University, operated by the Association of Universities for Research in Astronomy, Inc. under cooperative agreement with the National Science Foundation.

REFERENCES

Arp, H. 1964, ApJ, 139, 1045
Aumann, H. H., Fowler, J. W., & Melnick, M. 1989, AJ, 99, 1674
Baade, W., & Arp, H. 1964, ApJ, 139, 1027
Bohlin, R. C., Cornett, R. H., Hill, J. K., Hill, R. S., O'Connell, R. W., & Stecher, T. P. 1985, ApJ, 298, L37
Bothun, G. D., Lonsdale, C. J., & Rice, W. 1989, ApJ, 341, 129
Bothun, G. D., & Rogers, C. 1992, AJ, 103, 1484
Burstein, D., Bertola, F., Buson, L. M., Faber, S. M., & Lauer, T. R. 1988, ApJ, 328, 440
Cataloged Galaxies & Quasars Observed in the IRAS Survey 1985, prepared by C. J. Lonsdale, G. Helou, J. C. Good, and W. Rice (JPL, Washington, D.C.)
Ciardullo, R., Rubin, V. C., Jacoby, G. H., Ford, H. C., & Ford, Jr., W. K., 1988, AJ, 95, 438

Code, A. D., Welch, G. A., & Page, T. L. 1972, in The Scientific Results for the Orbiting Astronomical Observatory OAO-2(NASA SP-310), p. 559
Donas, J., Deharvang, J. M., Laget, M., & Huguenin, D. 1987, A&A, 180, 12
Devereux, N. A., & Scowen, P. A. 1994, AJ, 108, 1244
Devereux, N. A., & Young, J. S. 1990, ApJ, 350, L25
Devereux, N. A., & Young, J. S. 1991, ApJ, 371, 515
Devereux, N. A., & Young, J. S. 1992, AJ, 103, 1536
Devereux, N. A., & Young, J. S. 1993, AJ, 106, 948
Gavazzi, G., Cocito, A., & Vettolani, G. 1986, ApJ, 305, L15
Habing, H. J., *et al.* 1984, ApJ, 278, L59
Harwitt, M., Houck, J. R., Soifer, B. T., & Palumbo, G. G. C. 1987, ApJ, 315, 28
Helou, G., Soifer, B. T., & Rowan-Robinson, M. 1985, ApJ, 298, L7
Henderson, A. P. 1979, A&A, 75, 311
Israel, F. P., & Kennicutt, R. C. 1980, ApJ, 21, 1
Jacoby, G. H., Ford, H., & Ciardullo, R. 1985, ApJ, 290, 136
Kennicutt, Jr., R. C., 1992, ApJ, 388, 310
Kennicutt, Jr., R. C., & Kent, S. M. 1983, AJ, 88, 1094
King, I. R., *et al.* 1992, ApJ, 397, L35
Kodaira, K., Watanabe, T., Onaka, T., & Tanaka, W. 1990, ApJ, 363, 422
Lauer, T. R., *et al.* 1993, AJ, 106, 1436
Leech, K. J., Lawrence, A., Rowan-Robinson, M., Walker, D., & Penston, M. V. 1988, MNRAS, 231, 977
Lonsdale-Persson, C. J., & Helou, G. 1987, ApJ, 314, 513
Massey, P., Strobel, K., Barnes, J. V., & Anderson, E. 1988, ApJ, 328, 315
O'Connell, R. W., *et al.* 1992, ApJ, 395, L45
Pellet, A., Astier, N., Viale, A., Courtes, G., Maucherat, A., Monnet, G., & Simien, F. 1978, A&AS, 31, 439
Price, R., & Duric, N. 1992, ApJ, 401, 81
Rengarajan, T. N., & Verma, R. P. 1986, A&A, 165, 300
Rice, W., Boulanger, F., Viallefond, F., Soifer, B. T., & Freedman, W. L. 1990, ApJ, 358, 418
Rice, W., *et al.* 1988, ApJS, 68, 91
Romanishin, W. 1990, AJ, 100, 373
Rubin, V. C., & Ford, Jr., W. K., 1971, ApJ, 170, 25
Ryder, S. D., & Dopita, M. A. 1993, ApJS, 88, 415
Sanders, D. B., *et al.* 1986, ApJ, 305, L45
Sauvage, M., & Thuan, T. X. 1992, ApJ, 396, L69
Scowen, P. A., Dufour, R. J., & Hester, J. J. 1992, AJ, 104, 92
Smith, J. 1982, ApJ, 261, 463
Smith, B. J., Lester, D. F., Harvey, P. M., & Pogge, R. W. 1991, ApJ, 373, 66
Soifer, B. T., Rice, W. L., Mould, J. R., Gillett, F. C., Rowan-Robinson, M., & Habing, H. J. 1986, ApJ, 304, 651
Walterbos, R. A. M., & Braun, R. 1992, A&AS, 92, 625
Walterbos, R. A. M., & Braun, R. 1994, ApJ (in press)
Walterbos, R. A. M., & Schwering, P. B. W. 1987, A&A, 180, 27
Young, J. S., Kenney, J. D., Lord, S. D., & Schleorb, F. P. 1984, ApJ, 287, L65

1994AJ....108.1667D

M 31

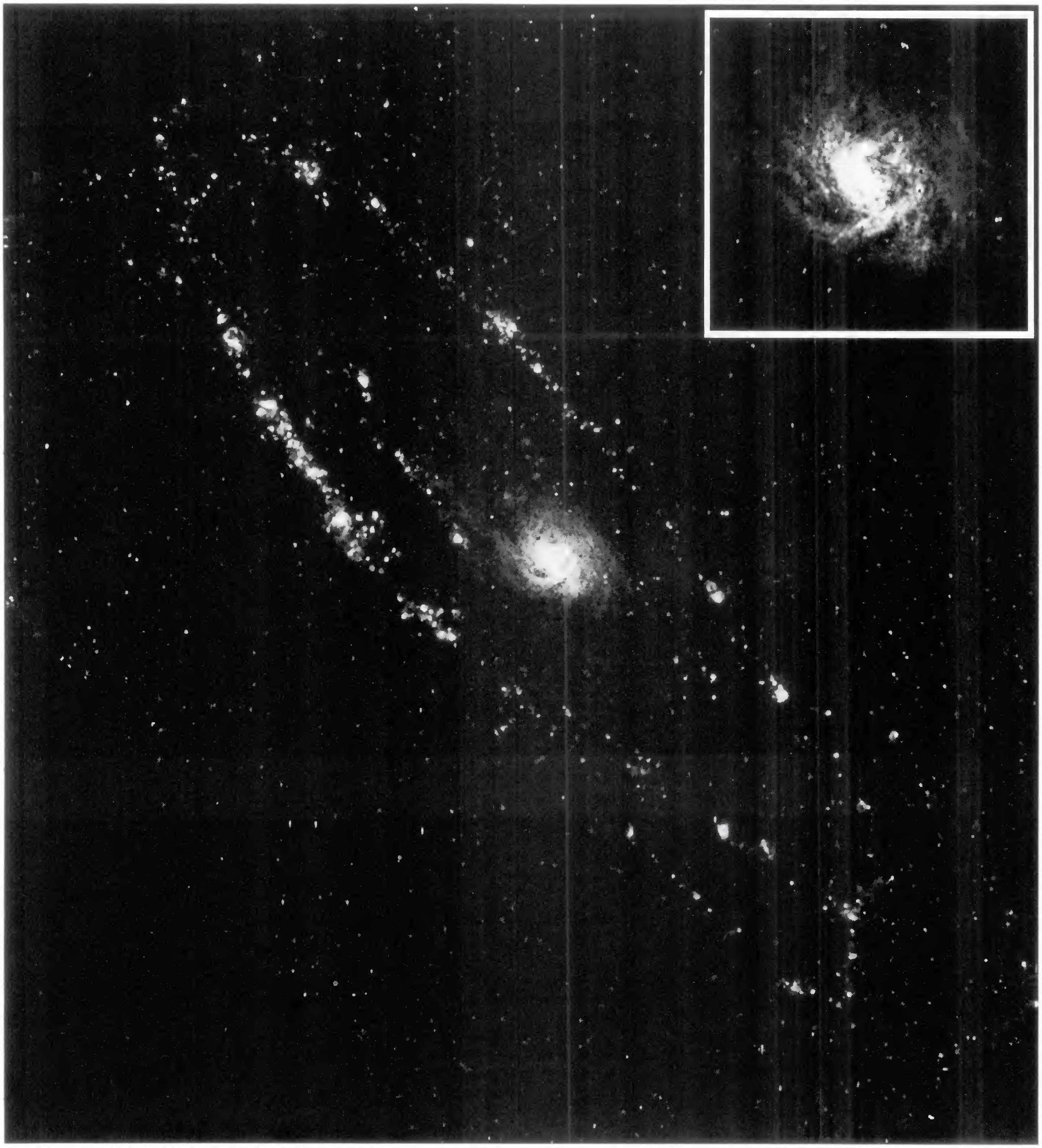

FIG. 1. Hα+[N II] image of M31. North is up, east to the left. The ring diameter is 1.65 degrees. Inset shows the nucleus magnified by a factor of 2.4.

Devereux *et al.* (see page 1668)

M 31

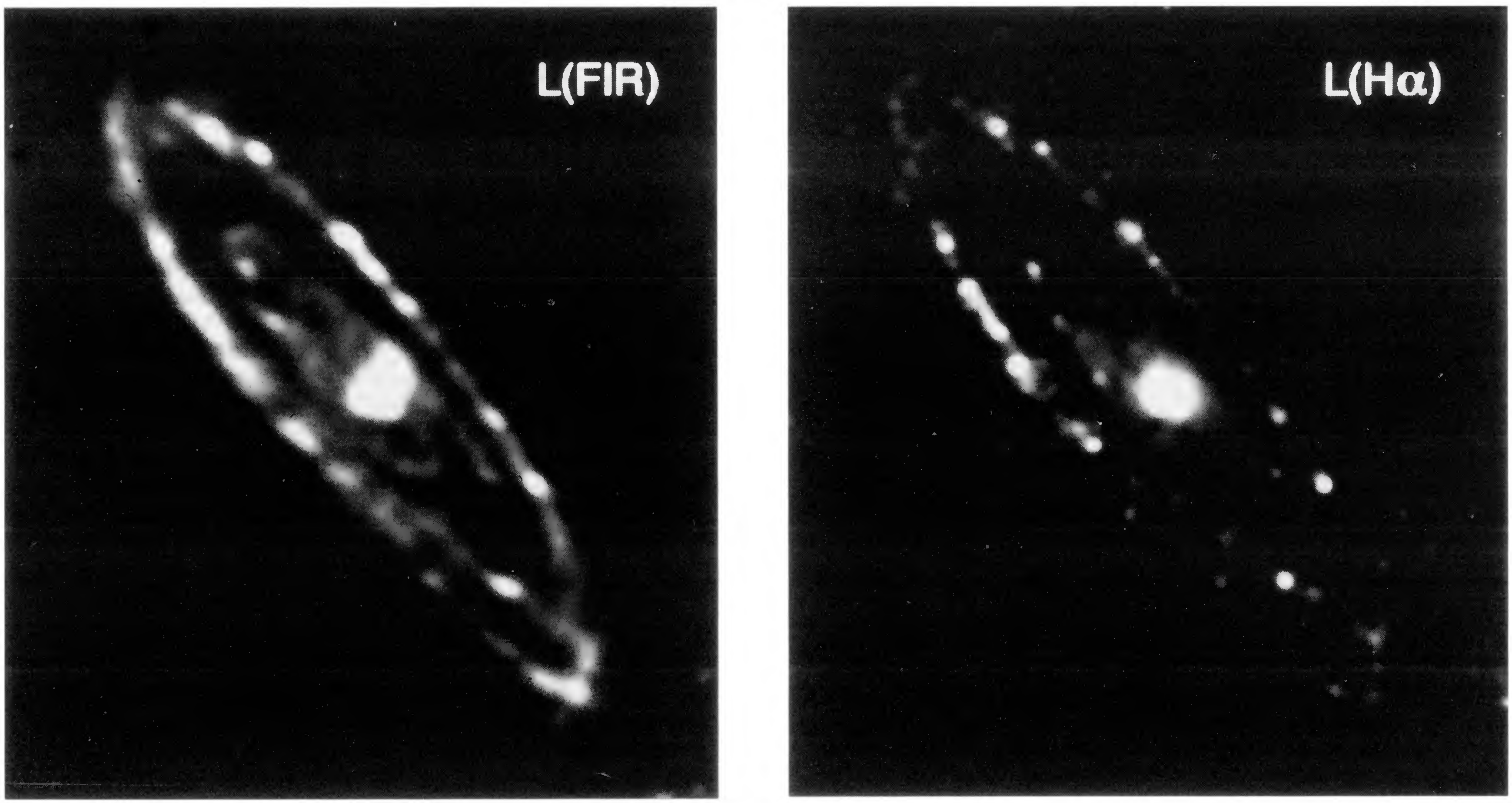

FIG. 2. (Left-hand panel). IRAS HiRes far-infrared image. (Right-hand panel) Hα image in Fig. 1 convolved to the same 105 arcsec resolution as the *IRAS* image. North is up, east to the left.

Devereux *et al.* (see page 1668)